Theory of Ultrafast Spin–Charge Quantum Dynamics in Strongly Correlated Systems Controlled by Femtosecond Photoexcitation: an Application to Insulating Antiferromagnetic Manganites

P. C. Lingos[1], M. D. Kapetanakis[2], M. Mootz[2], J. Wang[3], and I. E. Perakis[2,1]

[1] Department of Physics, University of Crete, Heraklion, Crete 71003, Greece and Institute of Electronic Structure and Laser, Foundation for Research and Technology-Hellas, Heraklion, Crete 71110, Greece

[2]Department of Physics, University of Alabama at Birmingham, Birmingham, Alabama 35294, U.S.A

[3]Ames Laboratory and Department of Physics and Astronomy, Iowa State University, Ames, Iowa 50011, U.S.A.

ABSTRACT

We use a non-equilibrium many-body theory that engages the elements of transient coherence, correlation, and nonlinearity to describe changes in the magnetic and electronic phases of strongly correlated systems induced by femtosecond nonlinear photoexcitation. Using a generalized tight–binding mean field approach based on Hubbard operators and including the coupling of the laser field, we describe a mechanism for simultaneous insulator–to–metal and anti– to ferro–magnetic transition to a transient state triggered by non–thermal ultrafast spin and charge coupled excitations. We demontrate, in particular, that photoexcitation of composite fermion quasiparticles induces quasi-instantaneous spin canting that quenches the energy gap of the antiferromagnetic insulator and acts as a nonadiabatic "initial condition" that triggers non-thermal lattice dynamics leading to an insulator to metal and antiferromagnetic (AFM) to ferromagnetic (FM) transitions. Our theoretical predictions are consistent with recent ultrafast pump-probe spectroscopy experiments that revealed a magnetic phase transition during 100fs laser pulse photoexcitation of the CE–type AFM insulating phase of colossal magnetoresistive manganites. In particular, experiment observes two distinct charge relaxation components, fs and ps, with nonlinear threshold dependence at a pump fluence threshold that coincides with that for femtosecond magnetization photoexcitation. Our theory attributes the correlation between femtosecond spin and charge nonlinearity leading to transition in the magnetic and electronic state to spin/charge/lattice coupling and laser-induced quantum spin canting that accompanies the driven population inversion between two quasi–particle bands with different properties: a mostly occupied polaronic band and a mostly empty metallic band, whose dispersion is determined by quantum spin canting.

Keywords: Quantum Femtosecond Magnetism, Femtosecond Magneto-optical Pump-Probe spectroscopy, Non-equilibrium Photoinduced Phase Transitions, Colossal Magnetoresistive Manganites, Ultrafast Magnetization Dynamics, Optical Control of Magnetic Properties

1. INTRODUCTION

The spin– and charge–ordered phases of quantum materials can be switched nonthermally by using strong laser pulses to initiate non–equilibrium phase changes during fs timescales. Non–equilibrium phase transitions can be triggered by laser–induced charge fluctuations[1,2] and by non–thermal populations of many–body states,[3] as well as by direct excitation of phonon oscillations. In this way, femtosecond (fs) laser pulses can initiate non–adiabatic time evolution via different electronic, magnetic, and lattice pathways that proceed in parallel. "Sudden" fs photoexcitation can create non-equilibrium transient states prior to the lattice thermalization that completes a

---

phase transition.[4, 5, 6, 7, 8] Metastable phases arise at pre-thermalization timescales of a few picoseconds. Ultrafast pump–probe or THz spectroscopy experiments can probe ultra-short times following strong pump photoexcitation and access the initial temporal regime that drives such non-equilibrium laser–induced phase transitions. This approach can be used to reveal metastable hidden phases prior to establishment of a new quasi–equilibrium lattice structure.

Fully time-dependent theoretical and computational approaches are required for addressing ultrafast spectroscopy experiments and for exploring non-thermal control schemes, including a quantum theory of coupled spin and charge dynamics in systems with deformable spin and lattice backgrounds. Such approaches suitable for addressing the non–equilibrium states observed in ultrafast spectroscopy experiments have lagged behind. Ginzburg-Landau equations, non-equilibrium dynamical mean field theory, density matrix renormalization group, time-dependent density functional theory, exact diagonalization, and canonical transformations all have advantages and disadvantages when modeling time-dependent quantum many-body problems. For example, while time-dependent density functional theory (TD-DFT) has successfully described molecular excitations, it faces difficulties when applied to extended systems with large unit cells. Moreover, TD-DFT is too expensive computationally when addressing time-dependent quantum many-body problems requiring hundreds of time steps and large super-cells containing hundreds to thousands of atoms as in the manganites. The close proximity of many phases and the complex unit cells with many atoms, as well as disorder, inhomogeneity, and lattice nonlinearities, limit the accuracy of ab initio methods when treating the phase competition away from equilibrium, especially during non-thermal timescales. Further, ab initio methods must include strong local correlations (e.g., LDA+U, LDA+DMFT) leading to strong spatial variations. Effective tight-binding models[9, 10] adequately describe energy bands close to the Fermi level, scale better for calculations of large systems, and access longer timescales. Tight-binding density-functional methods[9] can improve on the simpler models.

In semiconductors,[1, 2, 3] different theoretical methods have been developed that describe relaxation and correlation by using density matrices derived from effective Hamiltonians. In the pre-thermalization temporal regime of interest here, photo-induced lattice displacements prior to the establishment of a new equilibrium lattice structure change the electronic and magnetic structure. The latter is described to first approximation by using classical equations of motion, with forces determined by the electronic total energy, including contributions from non-thermal electronic and spin populations, as well as from lattice nonlinearities leading to metastability. A modeling and computational approach suitable for a large dynamic range in time is needed in order to provide experimentalists with an understanding of scaling and order parameters that lead to systematic understanding of the ultrafast response of widely varying Phase Changing Materials types. Such theory aims to describe non-thermal properties and metastable phases of quantum materials arising from many-body interactions initiated by femtosecond laser pulses. Model Hamiltonians studied with different theoretical techniques have been used to make progress in understanding strongly correlated systems.[11] There is still a great deal of research needed for theory to adequately describe observed experimental phenomena in phase changing materials.

Femtosecond nonlinearities are known to lead to non-adiabatic quantum dynamics in interacting electron-gas[3, 12] and exciton,[1, 2] many-body systems. While the well–studied femtosecond nonlinear response of semiconductor nanostructures is determined by many-body interactions of carriers in rigid energy bands, quasi-particle bands in quantum materials are soft and can thus be manipulated in different ways via ultrafast laser pulses. The relevant Hamiltonians incorporate strong local interactions: Hubbard-U, spin-exchange, and Jahn-Teller (JT) distortions. The time-dependence arises from quasi-instantaneous populations of photo-generated carriers and nonlinear couplings of the strong laser fields. Non–equilibrium methods for treating such quantum many body Hamiltonians can be generally subdivided into wave-function/density matrix and Greens function methods. Differences between these two approaches arise from the handling of time propagation in many-body systems. Non-equilibrium Greens functions require two time arguments, which strains computer memory and is very time consuming. Here we employ instead single-time density matrix methods and treat correlations explicitly, separating the density matrix into quasi-thermal and non-thermal parts.[7] The quasi-thermal component describes degrees of freedom that reach quasi–equilibrium on timescales shorter than the experimental resolution, while the non-thermal contribution is due to quantum kinetics of elementary excitations prior to thermalization. The time–dependent part of the Hamiltonian drives non-adiabatic dynamics that generate non-thermal phase competition and distinguishes fast from slow degrees of freedom. Ultrafast time dependence arises from quasi-instantaneous

coupling of quantum spin canting, charge fluctuations and correlations due to fs photo-excitation and quenching of electronic gap, as well by fast lattice displacements. To describe such effects, we employ effective tight-binding models that can describe bands close to the Fermi level, scale better for calculations of large systems, and permit access to longer timescales.

The physical properties of complex materials such as colossal magnetoresisitive manganites[13] are governed by collective order and fluctuations of coupled degrees of freedom.[14, 15, 16, 17, 18] This results in elementary excitations and order parameters with coupled charge, orbital, spin, and lattice components, whose precise microscopic composition remains unknown.[8, 19, 20, 21, 22, 23] In the manganites, while strong coupling of electronic, magnetic, and lattice degrees of freedom is believed to be responsible for the emergence of coexisting insulating/lattice–distorted/AFM and metallic/undistorted/FM nanoscale regions,[13] the relevant quasi–particles have not been fully characterized yet.[23] Some theoretical studies have proposed that the sensitivity to the non–thermal electronic perturbations leading to the CMR phase transition from AFM/insulating to FM/metallic state may be due to delocalized electrons with mobility mediated by classical spin–canting,[19, 24, 25] which coexist with the polaronic carriers that dominate in the insulating ground state.[26, 27, 28]

In such quantum materials, there are two possible pathways leading to a photo-induced phase transition:[29] (1) an electronic charge and spin pathway triggered by laser-induced sudden excitation of non-thermal spin and charge populations. Subsequent relaxation of the photoinduced electronic and spin populations also changes the energy landscape in the excited state, (2) a lattice pathway, which eventually leads to a delayed crystallographic phase transition that typically completes within ps timescales.[30] Here we are mostly interested in the first stage of the time–dependent process initiated by fs laser excitation of AFM insulating systems. In VO_2[29] and $TiSe_2$[8] systems, previous experiments have shown that quasi-instantaneous electronic processes induced by the photo–carriers lead to metastable states prior to an insulator–to–metal phase transition, where the electronic and lattice orders evolve differently.[8, 31] For example, in the $TiSe_2$ insulator, the electronic component of the charge density wave order parameter is quenched quasi-instantaneously while the lattice component persists.[8] This results in a non–equilibrium state with lattice order similar to equilibrium, whose properties are controlled by the photoinduced change in the local electronic density matrix.[8] In VO_2, a metastable metallic phase with the monoclinic lattice structure of the insulating phase is observed after the electronic component has switched from insulating to metallic.[31] So far, the role in such non–equilibrium photoinduced states of spin non–thermal fs dynamics is less understood. Here we discuss the role of spin fluctuations driven by photo–carrier populations that interact with a deformable spin and lattice medium.

In low-bandwidth insulating manganites such as the $Pr_{0.7}Ca_{0.3}MnO_3$ system (PCMO), metallic phases cannot be accessed by tuning the temperature.[13] An AFM insulator to FM metal equilibrium phase transition can, however, be induced non–thermally, e.g. by applying a strong magnetic field, which leads to CMR. While in equilibrium a magnetic field simultaneously changes the coupled electronic, magnetic, and lattice order components, several ultrafast spectroscopy experiments[17, 18, 32, 33, 34, 35, 36, 37, 38, 39, 40] have observed non–thermal charge and/or spin dynamics prior to electron–lattice relaxation. While a new lattice structure seems to be established after ps timescales, electronic, orbital, and magnetic orders have been observed to change much faster. Photo-induced non-equilibrium phase transitions are typically characterized by a nonlinear threshold dependence of the measured properties on the pump laser fluence. The time evolution of the charge, orbital, lattice, and magnetic components of a complex order parameter can be separately monitored with fs X-ray diffraction (XRD).[32, 33] The fs dynamics of AFM order is less understood, as it may involve an AFM→FM transition initiated by charge excitations. Ref.[4] reported a threshold increase of the fs-resolved magneto-optical Kerr and circular dichroism signals at 100fs time delays, which is absent at ps time delays and only appears below the AFM transition (Neel) temperature when a small magnetic field breaks the symmetry. This fs nonlinearity was interpreted in terms of an AFM→FM transition that occurs prior to the ps spin–lattice relaxation.[4] It was proposed that *quantum femtosecond magnetism*[6] and FM correlation may arise from both laser–driven charge fluctuations and non-thermal electronic populations. Here we discuss the microscopic link between spin and charge nonthermal excitations in the fs temporal regime.

A possible nonthermal mechanism for photoinduced phase transition is based on the interplay between a quasi–instantaneous electronic/magnetic quantum pathway and a lattice pathway. In particular, we discuss the possibility that the excitation of composite fermion itinerant quasi–particles dressed by spin fluctuations

triggers quasi–instantaneously an insulator to metal and AFM to FM phase transition. We discuss the role of the 'soft quasi–particle energy bands, modified by fs laser excitation, which arise from electron–magnon coupling and the strong Hund's rule local interaction. We note that electron–magnon quantum fluctuations have been observed experimentally to significantly change the spin–wave energy dispersion and lifetimes in metallic manganites.[41,42,43] For this purpose, we present a non-equilibrium modeling scheme based on quantum-kinetic equations of motion for the local electronic density matrix coupled to lattice displacements. Our emphasis here is on photo-induced quantum many-body dynamics of intertwined charge, spin and lattice orders that govern electronic, magnetic, and structural phase transitions in manganites. Such theory can facilitate discovery and identification of hidden metastable quantum phases and emergent order, which is accessed via laser-driven non-adiabatic pathways and quantum fluctuations. We use a generalized tight-binding approximation based on Hubbard operators,[21] with parameters can be taken from the manganite literature,[13,23] to investigate how local correlations affect quasi-particle spectra and collective spin behavior following ultrafast photo-excitation, by extending the semiconductor Bloch equations[1] to strongly correlated systems. We model coupled, non-thermal spin-charge dynamics for itinerant electrons hopping between clusters with localized electrons in well–defined spin states. We treat these localized electrons as core spins S with magnetic quantum numbers. Total spin is conserved during electronic motion and we separate the J=S+1/2 and J=S-1/2 Hubbard bands. Itinerant electrons preferentially form J=S+1/2 total spin states due to the strong Hund's rule interaction. Electron motion is then restricted and deforms the core AFM spin background via quantum fluctuations induced by spin-flip magnetic exchange interactions. We present numerical results for a CE–type AFM unit cell. Our calculations show strong coupling of the AFM chains and planes that characterize the insulating states of the manganites. In particular, quantum spin fluctuations induced by the charge excitations[13,23,25] delocalize the excited quasi–particles due to deformation of the AFM spin background during the electronic hopping. We show that this leads to a broad metallic conduction band and a quench of the insulator energy gap facilitated by photoinduced FM correlation. As a result, the critical value of the Jahn–Teller (JT) lattice displacement necessary for stabilizing an insulating state changes. Using the above results, we propose a theoretical description of ultrafast transition to a non–equilibrium metallic state with FM correlation and lattice displacements, which differs from equilibrium.

2. PROBLEM SETUP

An important characteristic of strongly correlated systems is the strong on–site local interactions, such as Coulomb, electron–phonon/Jahn–Teller, spin–exchange, etc– whose strength well–exceeds the kinetic energy bandwidth. To first approximation, strong local interactions restrict the population of the local electronic configurations thatare energetically unfavorable, which restricts the itinerant electron motion. Rather than describing the dynamics in terms of bare electron operators, as in weakly–coupled semiconductors and metals, we start from the atomic limit and the Hubbard picture.[44] In this picture, electronic motion arises from transitions between local many-electron configurations with given total spin. We thus consider a lattice of atomic clusters located at sites labeled by i. We use the basis of the atomic many–body states that diagonalize the local Hamiltonian at each lattice site. We assume that site i can be populated by either N or $N+1$ electrons, with the fluctuation in the population of the local configurations caused by an itinerant electron hopping from site to site or by laser photoexcitation. We assume that the atomic Hamiltonian of an "empty" site i (N localized electrons) has eigenstates $|im\rangle$, where $m = -S, \cdots S$ labels the z–component of a local spin S (S_z). The limit $S = 0$ corresponds to an empty site without local spin, while the limit $S \to \infty$ corresponds to a classically treated local spin. The local eigenstates at "full" sites populated by a single itinerant electron ($N+1$ total electrons) are labeled by $|i\alpha M\rangle$, where M is the z–component of the total spin $J_i = S_i + s_i$ formed by the itinerant and the N localized electron spins. Index α describes all other quantum numbers, such as different orbitals in the presence of local (Jahn–Teller) lattice distortions, different total angular momentum values, doubly–occupied states ($N+2$ electrons), etc. We impose the local constraint

$$\sum_m |im\rangle\langle im| + \sum_{\alpha M} |i\alpha M\rangle\langle i\alpha M| = 1 \tag{1}$$

at each individual site, which implies that only the population of the above local many–electron configurations can significantly change during the itinerant electron motion. In the manganites, for instance, the relevant "active"
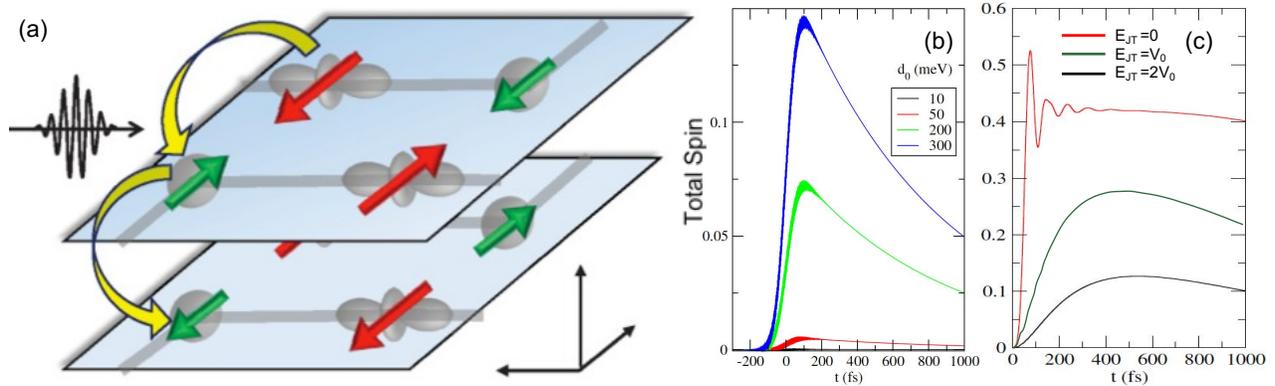
!

Figure 1. (a) Illustration of the intersite electronic excitations in the CE-AFM/CO/OO three–dimensional unit cell considered here, which consists of 16 sites in two stacked AFM planes and two AFM–coupled FM zigzag chains with alternating JT–distorted (bridge) and undistorted (corner) sites. (b–c) Calculated time–dependence of the total z–component $S_z(t)$ of the two AFM core spins discussed in the text, driven by the coupling of a 100-fs optical field pulse, for population lifetime $T_1 = 1$ ps and different Rabi energies d_0 (a), and (c) by the pulsed change in inter–site hopping amplitude discussed in the text. V_0=100meV.

Mn orbitals are the three–fold degenerate t_{2g}–orbitals and the partially–filled (or empty) doubly–degenerate e_g–orbitals while the neighboring oxygen atoms participate as well similarly to the Zhang–Rice local singlet between the O hole and Cu^{2+} ion in the Cu–oxide superconductors.[45] The most important configurations correspond to total spin $J=2$ in "bridge" sites ($|i\alpha M\rangle$) and $S \approx 3/2$ in "corner" sites ($|im\rangle$). The population of the two sites differs by ~ 1 in equilibrium, with the extra charge populating oxygen holes and e_g manganite orbitals. Moreover, the population of states with total spin $J = S-1/2$ is suppressed for strong Hund's rule ferromagnetic interaction $J_H \to \infty$ between the itinerant and local electron spins on a given site. Finally, the Jahn–Teller (JT) local deformation of MnO_6 octahedra lifts the local state degeneracy of the electronic states.[13, 46, 47]

Here we are mostly interested on the role of spin fluctuations in laser–induced insulator→metal and AFM→FM non–equilibrium phase transitions. Within classical spin scenarios, the itinerant electrons move on top of an adiabatically–decoupled spin background with their spins FM–locked to the localized electron spins at each site: $M=S+1/2$ and $m=S$. Such an adiabatic picture assumes that the electronic hopping fluctuations occur on a time scale faster than the spin dynamics. The local spins then point along the spin–canting angles θ_i, which define a local z–axis that varies from site to site and defines the quasi–equilibrium directions of the local spins that change adiuabatically, i.e. much slower that quantum spin and charge fluctuations. For an equilibrium state consisting of AFM–coupled chains with FM spin correlation, as in the CE–AFM state of Fig. 1(a), spin conservation then restricts the electronic motion for large J_H, due to the magnetic exchange energy cost for creating an anti–parallel spin configuration.[13] While such effects also determine the equilibrium properties, here we are interested in their pump–induced changes following strong pump photoexcitation of itinerant carriers. On the other hand, quantum spin fluctuations allow the non–equilibrium photoelectrons to hop on sites with anti–parallel spins by flipping the localized spins via $J_H S_i^{\pm} \cdot s_i^{\mp}$. They can then form states with $J = S+1/2$ but $M=S-1/2$ or smaller via electron–magnon quantum fluctuations.[41, 42, 43]

In the strongly correlated limit, we describe the electronic and spin excitations in terms of transitions between the above atomic many–body states, created by local "Hubbard operators". An example is the familiar Frenkel exciton operator,[48] which creates a transition between the ground state and e–h excited state of an atom. Excitations that conserve the total number of electrons are described in terms of the Hubbard operators

$$\hat{X}_i(m; m\prime) = |im\rangle\langle im'|, \hat{X}_i(\alpha M; \alpha' M') = |i\alpha M\rangle\langle i\alpha' M'|, \qquad (2)$$

which commute at two different lattice sites and satisfy bosonic–like non–canonical commutation relations. Our theory for the spin dynamics is based on quantum kinetic equations of motion for the density matrix ρ_i which is defined in terms of the populations of the local many–body states at each site i as follows:

$$\rho_i(m) = \langle |im\rangle\langle im| \rangle, \rho_i^\alpha(M) = \langle |i\alpha M\rangle\langle i\alpha M| \rangle. \tag{3}$$

Here we neglect photoinduced coherent couplings between the different local configurations α. The above–defined local density matrix is used here to describe the local spin at site i and its quantum dynamics. Neglecting the $J=S$-1/2 high energy configurations, the core spin component $S_z(i)$ along the local z–axis defined by the equilibrium spin canting angle θ_i may be expressed as follows:

$$S_z(i) = \sum_{m=-S}^{S} m\, \rho_i(m) + \sum_{M=-S-\frac{1}{2}}^{S+\frac{1}{2}} M\, \frac{S}{S+\frac{1}{2}} \sum_\alpha \rho_i^\alpha(M), \tag{4}$$

Similarly, the z–component of the itinerant electron spin is expressed as

$$s_z^\alpha(i) = \frac{1}{2S+1} \sum_{M=-S-\frac{1}{2}}^{S+\frac{1}{2}} M\, \rho_i^\alpha(M). \tag{5}$$

The z–axis of spin quantization refers to the equilibrium direction to which the spin relaxes on a given site. It therefore varies from site to site. The above expressions for the spin on site i were obtained after noting that the eigenstates of the magnetic exchange interaction $J_H \mathbf{S_i} \cdot \mathbf{s_i}$ coincide with the eigenstates of the total spin and, for $J = S+1/2$, are given by

$$|i\alpha M\rangle = \sqrt{\frac{S+M+\frac{1}{2}}{2S+1}}\ |i\alpha;\uparrow M-\frac{1}{2}\rangle + \sqrt{\frac{S-M+\frac{1}{2}}{2S+1}}\ |i\alpha;\downarrow M+\frac{1}{2}\rangle, \tag{6}$$

where $M=-J\cdots J$ and α labels the eigenstates of the JT and all other local interactions on site i. The above equation introduces the Glebsch-Gordan coefficients

$$F_\sigma(M) = \sqrt{\frac{S+\frac{1}{2}+\sigma M}{2S+1}}. \tag{7}$$

Here by neglecting all $J=S-1/2$ configurations, we do not include any spin dynamics on time scales of the order of the inverse magnetic exchange energy $\sim \hbar/J_H$, which is typically in the sub–femtosecond range. We thus neglect the effects of the upper magnetic Hubbard band. Instead, we describe spin dynamics driven by the off-diagonal spinflip interaction $J_H S_i^\pm \cdot s_i^\pm$, which couples the different M states with the same magnetic energy (quantum spin flucutations). In equilibrium, only the M=S+1/2 state is populated, similar to classical spins. However, as the photoexcited electrons hop from site to site by flipping the local spins and exciting low energy magnons, different spin configurations can be populated off–equilibrium. For example, a spin–$\uparrow$ electron can hop on an empty site with local spin pointing along the -z direction ($|i-S\rangle$ state) and form a $|i, \alpha, -S+1/2\rangle$ local configuration, Eq.(6), at zero magnetic energy cost. Such electron–magnon states are not allowed in the classical spin limit $S \to \infty$. Their effect on the femtosecond spin dynamics is treated non–perturbatively here.

The equations–of–motion for the local density matrix Eq.(3) at a given site i couple to neigboring inter–site coherences. The latter describe transient couplings of the atomic quantum states in two different lattice sites, which can be driven by the laser field or by ultrafast changes in the hopping amplitudes. To describe inter–site electron hopping in a deformable spin background in the presence of strong local correlations, we introduce 'composite fermion local electronic excitations created by Hubbard operators[21,44] that change the number of electrons by one and describe transitions between the active multi–electron configurations on a given site i:

$$\hat{e}_{\alpha\sigma}^\dagger(iM) = |i\alpha M\rangle\langle i, M-\frac{\sigma}{2}|, \tag{8}$$

where $\sigma=\pm 1$ labels the z–component of the local excitation total spin ($\hbar =1$). The above composite fermion operators create a total spin–$\sigma/2$ local excitation. The Hubbard operators obey the noncanonical anticommutation relations[21, 22]

$$[\hat{e}^{\dagger}_{\alpha'\sigma'}(i'M'), \hat{e}_{\alpha\sigma}(iM)]_{+} = \delta_{ii'}\left[\delta_{M',M+\frac{\sigma'-\sigma}{2}}\,|i\alpha'M'\rangle\langle i\alpha M| + \delta_{M',M}\,\delta_{\alpha,\alpha'}\,|i, M - \frac{\sigma}{2}\rangle\langle i, M' - \frac{\sigma'}{2}|\right]. \tag{9}$$

The difference of the composite fermion anticommutators from the usual fermion anticommutators is sometimes refered to as the "kinematic interaction" and arises from the strong local correlations that restrict the populations of the different atomic many–body states. We thus project the bare electron operators on the subspace of populated atomic states, Eq.(6), by using Eqs (4)–(5) and the Glebsch–Gordan coefficients Eq.(7) to obtain the projected Hamiltonian that conserves spin:

$$H(t) = \sum_{i}\sum_{\alpha M} E_i(\alpha M)\,|i\alpha M\rangle\langle i\alpha M| + \sum_{i}\sum_{m} E_i(m)\,|im\rangle\langle im| + H_{hop}, \tag{10}$$

The local excitation energies

$$\varepsilon_{\alpha\sigma}(i) = E_i(\alpha M) - E_i(M - \frac{\sigma}{2}), \tag{11}$$

depend on the lattice coordinates due to the electron–lattice (JT) local coupling, which lowers excitation energy, $\varepsilon_{\alpha\sigma}(i) = -E_{JT}(Q_i)$, where Q_i describes the local classical lattice distortion, while in all JT–undistorted sites, $\varepsilon_{\alpha\sigma}(i)=0$ if we neglect high energy electronic configurations α.

The quasi–particle inter–site hopping is described by[21]

$$H_{hop}(t) = -\sum_{ii'}\sum_{\sigma}\sum_{\alpha\alpha'} V_{\alpha\alpha'}(i - i')\left[\cos\left(\frac{\theta_i - \theta_{i'}}{2}\right)\hat{e}^{\dagger}_{\alpha\sigma}(i)\,\hat{e}_{\alpha'\sigma}(i') + \sigma\,\sin\left(\frac{\theta_i - \theta_{i'}}{2}\right)\hat{e}^{\dagger}_{\alpha\sigma}(i)\,\hat{e}_{\alpha'-\sigma}(i')\right] \tag{12}$$

where $\hat{e}^{\dagger}_{\alpha\sigma}(i) = \sum_M F_\sigma(M)\hat{e}^{\dagger}_{\alpha\sigma}(iM)$ and the amplitudes $V_{\alpha\alpha'}(i - i')$ have both static ($t_{\alpha\alpha'}$) and laser–induced ($\Delta V_{\alpha\alpha'}$) contributions, $V_{\alpha\alpha'}(j - i) = t_{\alpha\alpha'} + \Delta V_{\alpha\alpha'}(t)$. Importantly, Eq. (12) ensures conservation of total spin during electronic motion. Transient changes in the above inter–site hopping amplitudes, ΔV, can arise from either the direct coupling of the optical field or by photoinduced transient changes in the local lattice distortions Q and local many–electron configurations $|i\alpha M\rangle$. The above Hamiltonian is quite general and does not rely on the details of the local configurations at each site i. The latter determine the effective parameters $E_i(\alpha M)$ and $V_{\alpha\alpha'}(i - i')$, which can also be fitted from a more micrtoscopic theory.

In the classical spin limit, the only populated states have $m = S$ or $M = S + 1/2$, as all spins point along directions $\theta_i(t)$ that depend on the lattice site. Introducing the deviation of $S_z(i)$ from its classical value, $\Delta S_z(i) = S - S_z(i)$, and using the completeness relation Eq.(1) we obtain from Eq.(4)

$$\frac{\Delta S_z(i)}{S} = \sum_{\alpha}\sum_{M=-S-\frac{1}{2}}^{S-\frac{1}{2}} \frac{S + \frac{1}{2} - M}{S + \frac{1}{2}}\rho_i^{\alpha}(M) + \sum_{m=-S}^{S-1} \frac{S - m}{S}\rho_i(m). \tag{13}$$

The above equation describes canting from the classical spin direction θ_i due to the population of local states with $M \le S - 1/2$ and $m \le S - 1$ described by the local density matrix Eq.(3). Therefore, the femtosecond quantum kinetics of the local (onsite) density matrix driven by the coupling of the laser field pulse, described below, introduces local spin quantum dynamics that can lead to transient non–thermal changes in the magnetic interactions. Similarly, the local density matrix is used to describe the quantum fluctuations of the itinerant electron spin,

$$\Delta s_z^{\alpha}(i) = \frac{f_i^{\alpha}}{2} - s_z^{\alpha}(i) \tag{14}$$

where

$$f_i^{\alpha} = \sum_M \rho_i^{\alpha}(M), \tag{15}$$

is the electron charge population on site i, which describes the classical contribution.

We describe the non–thermal spin dynamics introduced by "sudden" laser excitations using quantum kinetic equations of motion for the spin–dependent local populations, obtained from Eq. (10):

$$
\begin{aligned}
\partial_t \rho_i^\alpha(M) &= 2\,Im \sum_{\sigma'=\pm 1} F_{\sigma'}(M) \times \sum_{l\alpha'} V_{\alpha'\alpha}(l-i) \times \\
&\quad \left\langle \left[\cos\left(\frac{\theta_l-\theta_i}{2}\right) \hat{e}^\dagger_{\alpha'\sigma'}(l) - \sigma' \sin\left(\frac{\theta_l-\theta_i}{2}\right) \hat{e}^\dagger_{\alpha'-\sigma'}(l) \right] \hat{e}_{\alpha\sigma'}(iM) \right\rangle \qquad (16)
\end{aligned}
$$

$$
\begin{aligned}
\partial_t \rho_i(m) &= -2 Im \sum_\alpha \sum_{\sigma'} F_{\sigma'}(m+\frac{\sigma'}{2}) \times \sum_{l\alpha'} V_{\alpha'\alpha}(l-i) \times \\
&\quad \left\langle \left[\cos\left(\frac{\theta_l-\theta_i}{2}\right) \hat{e}^\dagger_{\alpha'\sigma'}(l) - \sigma' \sin\left(\frac{\theta_l-\theta_i}{2}\right) \hat{e}^\dagger_{\alpha'-\sigma'}(l) \right] \hat{e}_{\alpha\sigma'}(i,m+\frac{\sigma'}{2}) \right\rangle. \qquad (17)
\end{aligned}
$$

The above equations describe the coupling of site i to the rest of the lattice, which is driven by $H_{hop}(t)$, Eq.(12). This time–dependent coupling is characterized by intersite coherent amplitudes $\langle \hat{e}^\dagger_{\beta\bar\sigma}(j)\,\hat{e}_{\alpha\sigma}(iM)\rangle$ describing spin–dependent charge fluctuations. The latter inter–site coherences are obtained from their equations of motion after using the factorization

$$
\langle [\hat{e}^\dagger_{\beta\bar\sigma}(j), \hat{e}_{\beta'\sigma'}(j)]_+ \hat{e}^\dagger_{\alpha'\sigma'}(l)\,\hat{e}_{\alpha\sigma}(iM)\rangle = \langle [\hat{e}^\dagger_{\beta\bar\sigma}(j), \hat{e}_{\beta'\sigma'}(j)]_+\rangle \langle \hat{e}^\dagger_{\alpha'\sigma'}(l)\,\hat{e}_{\alpha\sigma}(iM)\rangle, \qquad (18)
$$

where $j \neq l, i$. The above mean field approximation neglects any fluctuations in the composite fermion anticommutator $[\hat{e}^\dagger_{\beta\sigma}(j), \hat{e}_{\beta'\sigma'}(j)]_+$ as in the Hubbard–I approximation.[21,44] We thus obtain after some simple algebra the equation of motion describing the time–dependent coupling between site i and the rest of the lattce $j \neq i$[49]

$$
\begin{aligned}
&i\partial_t \langle \hat{e}^\dagger_{\beta\bar\sigma}(j)\,\hat{e}_{\alpha\sigma}(iM)\rangle - [\varepsilon_{\alpha\sigma}(i) - \varepsilon_{\beta\bar\sigma}(j)]\,\langle \hat{e}^\dagger_{\beta\bar\sigma}(j)\,\hat{e}_{\alpha\sigma}(iM)\rangle \\
&= F_\sigma(M)\,\langle [\hat{e}^\dagger_{\alpha\sigma}(iM), \hat{e}_{\alpha\sigma}(iM)]_+\rangle \sum_l \sum_{\beta'} V_{\alpha\beta'}(i-l)\,\sigma \sin\left(\frac{\theta_l-\theta_i}{2}\right)\,\langle \hat{e}^\dagger_{\beta\bar\sigma}(j)\,\hat{e}_{\beta'-\sigma}(l)\rangle \\
&\quad - F_\sigma(M)\,\langle [\hat{e}^\dagger_{\alpha\sigma}(iM), \hat{e}_{\alpha\sigma}(iM)]_+\rangle \sum_l \sum_{\beta'} V_{\alpha\beta'}(i-l)\,\cos\left(\frac{\theta_l-\theta_i}{2}\right)\,\langle \hat{e}^\dagger_{\beta\bar\sigma}(j)\,\hat{e}_{\beta'\sigma}(l)\rangle \\
&\quad + \langle [\hat{e}^\dagger_{\beta\bar\sigma}(j), \hat{e}_{\beta\bar\sigma}(j)]_+\rangle \sum_l \sum_{\alpha'} V_{\alpha'\beta}(l-j)\,\cos\left(\frac{\theta_l-\theta_j}{2}\right)\,\langle \hat{e}^\dagger_{\alpha'\bar\sigma}(l)\,\hat{e}_{\alpha\sigma}(iM)\rangle \\
&\quad - \langle [\hat{e}^\dagger_{\beta\bar\sigma}(j), \hat{e}_{\beta\bar\sigma}(j)]_+\rangle \sum_l \sum_{\alpha'} V_{\alpha'\beta'}(l-j)\,\bar\sigma \sin\left(\frac{\theta_l-\theta_j}{2}\right)\,\langle \hat{e}^\dagger_{\alpha'-\bar\sigma}(l)\,\hat{e}_{\alpha\sigma}(iM)\rangle. \qquad (19)
\end{aligned}
$$

Noting Eq.(9), the first two lines in the above equation describe the coupling to the local density matrix at site i. The last two lines describe coupling of site i to the rest of the lattice. The coherent long–range coupling between any two lattice sites $j \neq l$ due to itinerant electron motion is similarly described by the equation of motion

$$
\begin{aligned}
&i\partial_t \langle \hat{e}^\dagger_{\beta\bar\sigma}(j)\,\hat{e}_{\alpha\sigma}(l)\rangle - [\varepsilon_{\alpha\sigma}(l) - \varepsilon_{\beta\bar\sigma}(j)]\,\langle \hat{e}^\dagger_{\beta\bar\sigma}(j)\,\hat{e}_{\alpha\sigma}(l)\rangle \\
&= \langle [\hat{e}^\dagger_{\beta\bar\sigma}(j), \hat{e}_{\beta\bar\sigma}(j)]_+\rangle \sum_{l'} \sum_{\alpha'} V_{\alpha'\beta}(l'-j)\,\left\langle \left[\cos\left(\frac{\theta_{l'}-\theta_j}{2}\right) \hat{e}^\dagger_{\alpha'\bar\sigma}(l') - \bar\sigma \sin\left(\frac{\theta_{l'}-\theta_j}{2}\right) \hat{e}^\dagger_{\alpha'-\bar\sigma}(l') \right] \hat{e}_{\alpha\sigma}(l)\right\rangle \\
&\quad - \langle [\hat{e}^\dagger_{\alpha\sigma}(l), \hat{e}_{\alpha\sigma}(l)]_+\rangle \sum_{l'} \sum_{\beta'} V_{\alpha\beta'}(l-l')\,\left\langle \hat{e}^\dagger_{\beta\bar\sigma}(j)\left[\cos\left(\frac{\theta_{l'}-\theta_l}{2}\right) \hat{e}_{\beta'\sigma}(l') - \sigma \sin\left(\frac{\theta_{l'}-\theta_l}{2}\right) \hat{e}_{\beta'-\sigma}(l') \right]\right\rangle \quad (20)
\end{aligned}
$$

The above equations of motion provide a closed system for describing the laser–induced nonthermal time evolution of the local density matrix and spins. They also describe time–dependent chaNges in the effective inter–site magnetic interactions mediated by ultrafast charge fluctuations driven by the laser field or by photoinduced ultrafast "sudden" changes in the effective local excitation energies and inter–site hoppings ("bonding order").

In the next section we discuss how short–range FM correlation can be transiently modified away from equilibrium by laser–induced charge fluctutations across the JT energy barrier..

The main difference between bare electrons and the composite fermion quasi–particles considered here comes from the spin–dependent anti–commutators

$$n_{\alpha\sigma}(i) = \langle [\hat{e}^\dagger_{\alpha\sigma}(i), \hat{e}_{\alpha\sigma}(i)]_+ \rangle. \tag{21}$$

The latter deviate from their fermionic values due to the strong local correlations, here the suppression of the population of $J=S-1/2$ total spin configurations during the electronic motion. Using the completeness relation Eq.(1) and Eqs.(4) and (5), we obtain

$$n_{\alpha\sigma}(i) = \frac{1}{2S+1}\left[S + \frac{1}{2} + \sigma\left(S_z(i) + s_z^\alpha(i) + \frac{\sigma}{2}\left(1 - f_i^\alpha\right)\right)\right]. \tag{22}$$

Introducing the quantum spin fluctuations, $\Delta J_z^\alpha(i) = \Delta S_z(i) + \Delta s_z^\alpha(i)$, Eqs. (13) and (14), we obtain from the above equation

$$n_{\alpha\sigma}(i) = \frac{S + \frac{1}{2} + \sigma\left(S + \frac{1}{2} - \Delta J_z^\alpha\right)}{2S+1} + \frac{1-\sigma}{2}\frac{1 - f_i^\alpha}{2S+1}. \tag{23}$$

In the limit of classical spins, $S \to \infty$, Eq.(23) gives $n_{\alpha\uparrow}(i) = 1$ and $n_{\alpha\downarrow}(i) = 0$ as in the case of bare electrons. In this approximation, the electrons are effectively spinless, as their spin is locked with the core spins during their motion, in a FM configuration parallel to θ_i due to Hund's rule.[13,50] On the other hand, in the case of composite fermions, Eq.(23) gives

$$n_{\alpha\uparrow}(i) = 1 - \frac{\Delta J_z^\alpha}{2S+1} \ , \ n_{\alpha\downarrow}(i) = \frac{1 - f_i^\alpha + \Delta J_z^\alpha}{2S+1} \neq 0, \tag{24}$$

which allows for σ=-1 quasi–particle excitations with total spin anti–parallel to the equilibrium spin direction θ_i. In the above equation, the composite fermion anticommutators depend on the local spin fluctuations ΔJ_z^α, as well as the filling factors f_i^α that determine the spatial modulation of the local charge.

3. LASER–DRIVEN FERROMAGNETIC CORRELATION: FEMTOSECOND QUANTUM SPIN DYNAMICS

In this section we discuss an example of how laser–induced charge fluctuations can quasi–instantaneously excite spin dynamics and short–range FM correlation between AFM sites based on quantum spin flucutations. To illustrate this possibility, we consider a "quantum dimer" of AFM local spins, which consists of a JT–distorted site (site 1) populated in the equilibrium state by a $J=S+1/2$ configuration $|i\alpha M\rangle$ with total spin M=S+1/2 and energy $-E_{JT}$, and an undistorted site (site 2) populated by a total core spin S with z–component m=$-S$ anti–parallel to the spin at site 1 and energy zero (see Fig. 2(a)). We assume that the optical field induces an ultrafast change in the intersite hopping amplitude V from its equilibrium value. Such time–dependent change in the hopping amplitude can be directly driven by the coupling of the optical field, which induces charge fluctuations between the two sites. However, it can also come from the excitation of non–thermal populations that change the local multi–electron configurations, by introducing, e.g., non–thermal lattice distortions that last during 100fs non–thermal time scales and proportional to the non–thermal electronic populations as discussed below.[51] The approximation of fairly localized charge density[52] simplifies the calculation and already captures some of the properties of the extended system.[23,24,53] It leads to an effective Hamiltonian with short–ranged interactions.[23,24,25] Here, such interactions are modified by any time–dependent pulsed change in the hopping amplitude, which drives inter–site non–equilibrium charge fluctuations as illustrated by the dash-lined arrow in Fig. 2(b). Such charge fluctuations result in laser–induced non–equilibrium changes in the local density matrix, which also affect the itinerant quasi–particle dispersion, energy bandgap, and phonon properties in correlated systems with "soft" energy bands. Previous examples include $TiSe_2$[8] or VO_2.[54] We solve the quantum–kinetic equations of motion for the spin–dependent density matrix of the two sites and then calculate the z–component of the total core spin of the two above sites, S_z=$S_z(1)+S_z(2)$, by using Eq.(4). We consider the same z–axis

for both sites. The local populations are assumed to relax on a timescale T_1=1ps, with the inter–site charge fluctuations dephasing on a timescale T_2= 50fs. However, the precise values of T_1 and T_2 do not change the qualitative behavior. Fig.1 compares the results for two different cases: (1) Optical field $\Delta V = V_0 e^{-(t/\tau)^2} e^{-i\omega t}$, (2) Pulsed change $\Delta V = V_0(1 - e^{-t/\tau_1}) e^{-t/\tau_2}$, with τ_1=100fs and τ_2=500fs. In the latter case, we compare the time–dependence for E_{JT}=0, V_0, and =2 V_0. E_{JT}=0 corresponds to hopping between two sites with the same lattice distortion, as is the case for hopping between two neighboring AFM planes with the same lattice and charge configurations, while $E_{JT} > 0$ corresponds to hopping between a JT–distorted and undistorted sites. Fig. 1(b) shows that a finite $\Delta S_z(t)$ develops with time, which corresponds to a photoinduced FM correlation induced by the quantum spin fluctuations. Note that, for classical spins, charge fluctuations between the two AFM sites are prohibited for $J_H \rightarrow \infty$ considered here, so any spin dynamics is adiabatic, determined by quasi–thermal changes in the local canting angles θ_i that describe the spin background adiabatically decoupled from the electronic motion. A long–range magnetization could then arise if a macroscopic number of such dimers (or clusters) orients along a preferred direction.[4,35,55] As seen in Fig. (1), in all cases the total spin $\Delta S_z(t) = \Delta S_z(1) + \Delta S_z(2)$ increases with time during the pulsed non–equilibrium change in the inter–site hopping amplitude from its ground state value.

To interpret the calculated time–dependence $\Delta S_z(t)$, we calculate all photoinduced populations $\Delta\langle|im\rangle\langle im|\rangle$ and $\Delta\langle|i\alpha M\rangle\langle i\alpha M|\rangle$ of the two sites as function of time. We note in Fig. (2) that the population of the M=S+1/2 site 1 ground state configuration decreases with time due to the laser–driven electron hopping to site 2, which creates a quasi–hole excitation $|1\alpha, S + 1/2\rangle \rightarrow |1S\rangle$ on site 1. This excitation leaves the core spin unchanged with m=S, so $\Delta S_z(1) \approx 0$. The electron hops to site 2 while conserving spin, by creating a local excitation $|2, -S\rangle \rightarrow |2\alpha, -(S-1/2)\rangle$. The population of these $M = -(S-1/2)$ configurations on site 2 results in quantum canting of the local spin $\Delta S_z(2) \neq 0$. For very short dephasing times, the charge fluctuations terminate after the initial charge transfer. For longer T_2, there are additional populations of other spin states, which which further enhances ΔS_z In this case, the photo–electron can hop back to site 1 from site 2 before the laser–induced inter–site coherence is destroyed, which can lead to non–equilibrium molecular bonding between AFM sites that modifies the inter–site magnetic exchange interaction. In all cases, charge photoexcitation induces quantum dynamics of $\Delta S_z(t)$, which increases from zero during electron hopping (quasi–instantaneous FM correlation). $\Delta S_z(t)$ describes non–adiabatic dynamics of the background spins, which leads to spin–canting from the quasi–equilibrium directions θ_i that is driven by the photoexcitation of quasi–particles dressed by spin fluctuations as discussed next.

4. DEPENDENCE OF ITINERANT QUASI–PARTICLE BANDS ON SPIN FLUCTUATIONS

In this section we discuss the effects of changes in the lattice potential and spin canting induced by the laser excitation and their possible implications for a non–equilibrium phase transition. Similar to previous works, we assume that the lattice motion can be described by classical coordinates Q.[13,24,25] The eigenstates $|i\alpha M\rangle$ of the local Hamiltonian depend on Q. We model the effects of electron–lattice coupling by introducing a linear Q–dependence of the energy eigenvalues $E_i(\alpha M)$ similar to Refs.[13,56] and neglect any changes in the hopping parameters, which are less known in the real materials.[23]

Eq.(20) suggests a Hubbard–I approximation for describing the itinerant quasi–particles:[21,44]

$$\omega_n \hat{e}_{\alpha\sigma}(i) = \varepsilon_{\alpha\sigma}(i) \hat{e}_{\alpha\sigma}(i)$$
$$-n_{\alpha\sigma}(i) \sum_l \sum_{\beta'} V_{\alpha\beta'}(i-l) \left[\cos\left(\frac{\theta_l - \theta_i}{2}\right) \hat{e}_{\beta'\sigma}(l,t) - \sigma \sin\left(\frac{\theta_l - \theta_i}{2}\right) \hat{e}_{\beta'-\sigma}(l,t)\right]. \tag{25}$$

Introducing the normal modes

$$\hat{e}_n = \sum_{i\beta\sigma} u_n^\sigma(i\alpha) \frac{\hat{e}_\sigma(i\beta)}{\sqrt{n_{\beta\sigma}(i)}}, \tag{26}$$
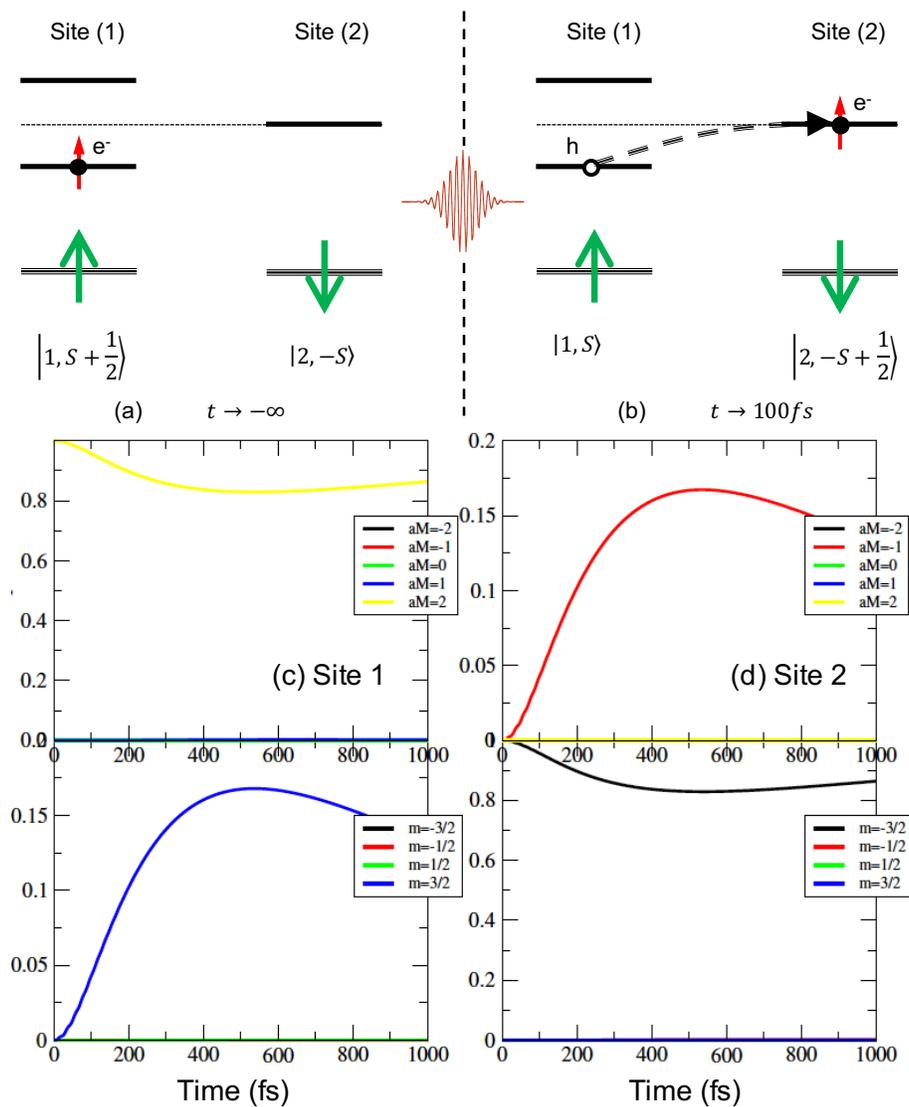
Figure 2. (a)–(b) Schematic of the dimer system before (a) and after (b) being driven by the optical field. (c)–(d) Time evolution of all photoinduced populations at the two sites of the dimer system.

where n labels the different quasi–particle branches (bands), we obtain from Eq. (25) the following eigenvalue equation that gives the itinerant quasi–particle energy bands:

$$\left(\omega_n - \varepsilon_{\beta\sigma}(j)\right) u_n^\sigma(j\beta) = -\sum_{l\alpha} V_{\alpha\beta}(l-j) \sqrt{n_{\beta\sigma}(j)} \sqrt{n_{\alpha\sigma}(l)} \cos\left(\frac{\theta_l - \theta_j}{2}\right) u_n^\sigma(l\alpha)$$

$$+\sigma \sum_{l\alpha} V_{\alpha\beta}(l-j) \sqrt{n_{\beta\sigma}(j)} \sqrt{n_{\alpha-\sigma}(l)} \sin\left(\frac{\theta_l - \theta_j}{2}\right) u_n^{-\sigma}(l\alpha). \tag{27}$$

The above eigenvalue equation couples σ=1 (parallel quasi–particle spin) and σ=-1 (anti–parallel quasi–particle spin) excitations (second line). By neglecting this coupling, the σ=1 contribution recovers the previous results for bare electrons and parallel classical spins.[13, 24, 50, 57] In this case, the quasi–particle spin is locked parallel to the background spins throughout the motion and the hopping amplitudes $V_{\alpha\beta}(l-j) \sqrt{n_{\beta\uparrow}(j) n_{\alpha\uparrow}(l)} \cos\left(\frac{\theta_l - \theta_j}{2}\right)$ are maximized between FM sites with $\theta_i = \theta_j$. On the other hand, for quantum spins, the finite $n_{\alpha\downarrow}(i)$ couples σ=1 and σ=-1 excitations and allows composite fermion quasi–particles to hop between AFM sites $|\theta_l - \theta_j| \sim \pi$. In this way, the quantum spin fluctuations couple the AFM chains and planes of Fig. (1)(a) (second term on the rhs of Eq.(27)) and lead to quasi–particle delocalization that strongly affect the energy bands. The results of this calculation are shown in Fig. (3), which compares the effects of quantum spin fluctuations with the energy bands obtained in the case of an adiabatic spin background that does not deform during the electronic motion (classical spin limit). The results of Fig. (3) were obtained with a real space calculation of a system with periodic boundary conditions, which converges for sufficiently large system size and reproduces the results obtained by assuming a periodic lattice. We consider the CE–AFM unit cell, shown in Fig. 1(a), with two AFM–coupled zig–zag chains that consist of two JT–distorted bridge sites and two undistorted corner sites with two orbitals.[13] Two AFM–coupled planes as in Fig. 1(a) have identical charge, lattice, and orbital configurations. While the "valence band" that is occupied in the insulating ground state is not strongly affected by quantum spin flucutations, Fig. (3) shows that the "conduction band" broadens significantly as a result of the added electronic delocalization between AFM chains and planes that is suppressed for classical (non–defomrable) spins. Eq.(27) thus describes "soft" energy bands of itinerant composite fermion quasi–particles, which depend non–perturbatively on the local spin and charge populations of the different lattice sites. In addition, the quasi–particle energy bands depend on the background spins via the classical spin–canting angles θ_i, whose effects are shown in Fig. (3). Finally, the energy bands depend on the classical lattice displacements Q and their dynamics, which determine the eigenstates $|i\alpha M\rangle$ on each lattice site and lead to lattice–dependent local excitation energies $\varepsilon_{\alpha\sigma}(i)$, Eq. (11). Fig. (3) shows that the "valence band" depends strongly on the JT energy gap, unlike for the conduction band. As a result, the insulating gap increases with JT lattice deformation but decreases due to spin canting, which results in two competing effects that affect differently the "conduction" and "valence" bands. In the next sections we discuss the possible role of such "soft" quasi–particle energy bands in photo–induced phase transitions.

4.1 Dependence of Quasiparticle Excitations on Lattice and Spin Dynamics

Fig. (3) shows the dependence of the low energy quasi–particle energy bands on the JT energy barrier $E_{JT}(Q) = \varepsilon_{JT}Q$ between JT–distorted bridge sites and undistorted corner sites, which populate zig–zag AFM–coupled chains in neighboring AFM planes. We compare the band Q–dependence between bare electrons, which move on top of an adiabatic classical spin background (upper panel), and composite fermion quasi–particles (lower panel), whose motion deforms the background spins.

The main feature demonstrated by Fig. (3) is that the conduction and valence bands have different dependence on both lattice distortions and spin fluctuations. As seen in Fig. (3), the energy gap is smaller in the case of deformable quantum spins, while it increases with lattice distortion Q. In the ground state, the system is insulating, so $Q > Q_c$ is required in the case of quantum spins, with Q_c been the critical displacement where the band gap closes. For classical spins (adibatic non–deformable spin background), the upper panel of Fig. (3) reproduces previous results.[24] For collinear CE–AFM order θ=0, in this case the energy gap does not close even for undistorted lattice Q=0 due to the electronic order of a single zig–zag chain.[13, 24] In the case of classical spins, Fig. 3(a) shows that the lowest conduction band state is a discrete degenerate state with energy $\varepsilon = 0$. The latter is a linear superposition of the electronic configurations in the two different corner sites of the zig–zag
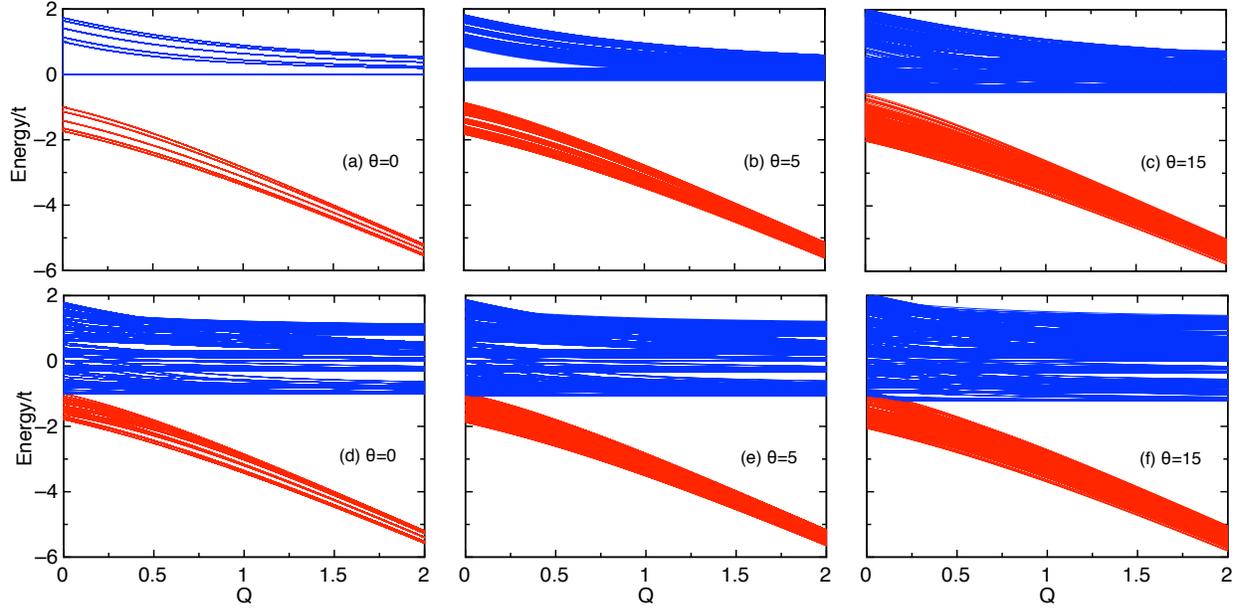
Figure 3. Calculated energy levels as function of lattice displacement, $E_{JT}=\varepsilon_{JT}Q$, for different spin canting angles θ, which describe FM correlation between the FM chains and planes with respect to the collinear AFM state $\theta=0$. Upper panel: Bare electrons (adiabatic spins, $S \to \infty$). Lower panel: Composite fermion quasi–particles (strongly–coupled quantum spins, $S=3/2$). $\varepsilon_{JT} = 2.5t_0$.

chain unit cell and thus does not depend on lattice deformation Q.[24] This is unlike for the valence band, which has strong contributions from the JT–deformed bridge sites. With increasing spin canting angle θ between the AFM chains, electronic hopping between planes breaks the degeneracy of the above $\varepsilon=0$ state, which broadens into the lowest conduction band.[24] For large FM correlation between the chains, $\theta \sim 15^o$, the energy gap closes, which results in metallic behavior induced by spin canting.

To compare with the above classical spin results, the lower panel of Fig. (3) shows that, with $n_\downarrow \neq 0$, the conduction band of composite fermion quasi–particles is already very broad and metallic in the collinear AFM ground state $\theta=0$. Such metallic conduction band arises from the quantum spin canting induced by the excitation of quasi–electron population in the conduction band that is mostly empty in the insulating AFM equilibrium state. Such conduction electrons can tunnel between the different AFM planes and chains due to electron–magnon quantum fluctuations that cant the background spins. The insulating state requires a finite JT lattice displacement $Q \neq 0$ to obtain a finite excitation energy gap. In this case, the valence band is full in equilibrium while the conduction band is mostly empty. Therefore, quantum spin fluctuations are not very pronounced in equilibrium, as can be seen by the small overall difference in the valence band between classical and quantum spins in the above figure. While treating the spin background as adiabatic assumes that it is slower than the electronic hopping, for composite fermions quantum spin canting occurs during electronic hopping timescales. This results in instantaneous metallic behavior and FM correlation during quasi–particle excitation even for large Q, which, as seen in Fig. 3(d), can quench the energy gap prior to any increase in θ. With increasing FM correlation between the chains, $\theta > 0$, the value of the critical lattice distortion $Q_c > 0$ below which the energy gap closes increases. Figs. 3(d), (e), and (f) suggest that an insulator to metal transition will occur when $Q \leq Q_c$.

In the case of composite fermions, the charge excitation gap depends on the spin fluctuations around the average direction $\theta_i(t)$, $\Delta J_z(i) = \Delta S_z(i) + \Delta s_z(i)$, given by Eqs. (13) and (14). The latter spin fluctuations can be induced by nonadiabatic photoexcitation of local spin populations with $M \leq S - 1/2$ and $m \leq S - 1$, which results in time–dependent changes of the composite fermion anti–commutator Eq.(24) and to quasi–instantaneous
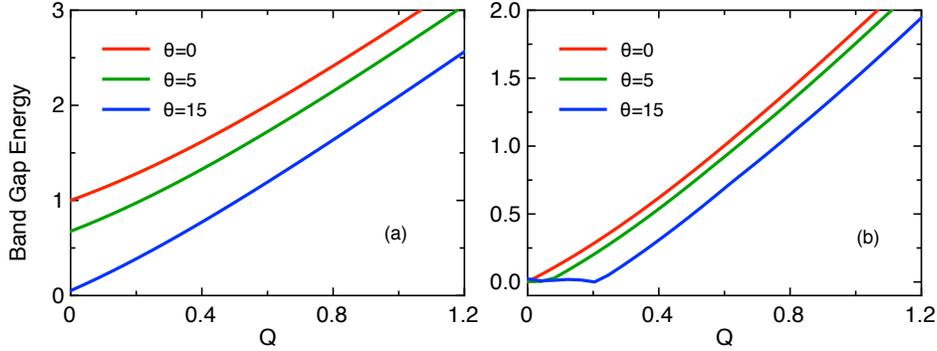
Figure 4. Effect of spin canting on the lattice dependence of the energy gap of Fig. (3) for increasing θ. (a) bare electrons, (b) composite fermion quasi–particles.

non–perturbative changes in the quasi–particle properties and energy dispersion, obtained from Eq. (24):

$$\Delta n_{\alpha\sigma}(i) = -\frac{\sigma\Delta J_z^\alpha(i) + \frac{1-\sigma}{2}\Delta f_i^\alpha}{2S+1} \tag{28}$$

Fig. (4) demonstrates an important difference in the Q–dependence of the e–h quasi–particle energy gap, extracted from Fig. (3), between composite fermion and bare electron excitations. In the case of bare electrons, Fig. 4(a), the energy gap does not close down to $Q=0$ without a large canting angle θ between the AFM chains. On the other hand, for composite fermions, Fig. 4(b) shows that quantum spin canting during quasi–particle excitation softens the energy gap, which now closes below $Q=Q_c \geq 0$ even for θ=0. Fig. (4) demonstrates the effect of the classical spin canting, which can be induced, e.g., by an external magnetic field or by fs laser excitation and results in an increase in the critical lattice displacement Q_c needed to maintain an insulating state. The critical value Q_c increases with background spin canting θ for both classical and quantum spins. However, in the case of bare electrons and assuming adiabatically–decoupled slower background spins and thus more "rigid" quasi–particle bands, a large spin canting angle θ is required for Q_c to be comparable to that of composite fermions with "soft" energy bands. As a result, the insulating state is less robust and rigid in the case of itinerant electrons moving on top of a deformable spin background (quantum spins).

As discussed in the previous section, laser excitation can result in photoinduced FM correlation $\Delta J_z(i) \neq 0$. In Fig. (5) we examine the effect of such spin fluctuations on the energy band gap for various values of the JT splitting between JT–distorted and undistorted sites. The dependence of the composite fermion anti–commutator $n_{\alpha\downarrow}(i)$ on the spin fluctuations $\Delta J_z^\alpha(i)$, which can be introduced by the photoexcitation, results in a dynamic change of the "soft" quasi–particle energy bands and the insulator bandgap already during time evolution of the spin populations and local density matrix, determined by the equations of motion Eqs.(17) and (16). In all cases, photoexcitation of $\Delta J_z^\alpha(i) > 0$ increases $n_{\alpha\downarrow}(i)$, which instantaneously quenches the energy gap and increases $Q_c(t)$ as shown in Fig. 5(a). Finally, by comparing the results for decreasing JT energy barrier in Fig. 5, we see that the effect of spin fluctuations on the itinerant quasi–particle motion diminishes as the JT splitting increases and becomes negligible in the deep insulating limit as shown in Fig. 5(c). Most importantly, Fig. 5(b) shows that in the realistic system with "soft" quasi–particle bands and JT energy barrier comparable to the electronic hopping energy, quantum spin fluctuations significantly affect the metal–insulator transition, which now requires larger lattice displacements following FM spin photoexcitation.

We conclude that, independent of the details of fs spin photogeneration, both adiabatic $\theta(t) > 0$ and nonadiabatic $\Delta J_z(t) > 0$ FM correlation induced by the photoexcited quasi–particles enhances the critical JT displacement $Q_c(t)$ required for insulator to metal transition when the lattice displacement $Q(t) \leq Q_c(t)$. This change in $Q_c(t)$ may already occur during photoexcitation of sufficient population of composite fermion quasi–particles, which leads to instantaneous FM correlation due to quantum spin fluctuations that quenches the insulator electronic energy gap. The detailed time–dependence of the photoinduced spin canting in different materials, which
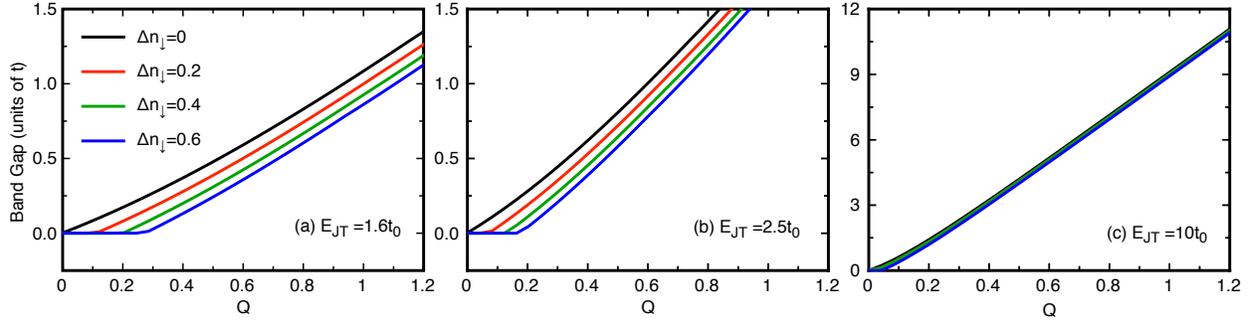
Figure 5. Effect of FM correlation on the lattice dependence of the energy gap. Composite fermion quasiparticles, increasing ΔJ_z. (a) $\varepsilon_{JT} = 1.6t_0$, (b) $\varepsilon_{JT} = 2.5t_0$, (c) $\varepsilon_{JT} = 10t_0$

determines the critical photocarrier density such that $Q(t) < Q_c(t)$ as required for a phase transition, depends on the details of the material, which are not well known. In all cases, Figs (4) and (5) imply a nonlinear dependence of the electronic properties on the pump fluence, as the latter controls the non–thermal populations of the composite fermion excitations that "suddenly" change the "soft" energy bands and $Q_c(t)$, while also inducing lattice displacements $Q(t) < Q$ as discussed next. We expect that, with multiple quasi–particle excitations, such nonlinear dependence will be even stronger than the single quasi–particle results presented here. We also note that classical spin equilibrium calculations[24] predict a very high critical magnetic field for inducing a CMR phase transition, due to the large charge excitation energy gap for adiabatically–decoupled spins. Here we argue that composite fermion excitations characterized by "soft" energy bands that can be manipulated optically can make an insulator to metal and AFM to FM transition possible for low magnetic fields and pump fluences.

4.2 Photoinduced softening of the lattice displacement

As discussed in the previous section, photoexcitation can induce an insulator–to–metal transition by changing the lattice displacement ib equilibrium, $Q > Q_c$, to $Q(t) \leq Q_c(t)$. This can be achieved in two different ways: (i) increase critical displacement $Q_c(t) > Q_c$, (ii) decrease in lattice displacement $Q(t) < Q$. In this section we explore the second possibility during nonthermal fs timescales. The effective potential that governs the lattice motion leading to $Q(t)$ includes both the classical contribution $U_L(Q)$, which can be obtained phenomenologically based on the symmetry,[32,58] and the contribution of the local electron–lattice coupling. The latter is important for the laser–induced phase transition proposed here and is described by the Q–dependence of the Hamiltonian Eq.(10). The lattice equations of motion can be derived as in Ref.[49,59] For this we introduce an orthogononal basis of many–electron ground state $|G\rangle$ excited states $|E\rangle$ of $H(Q)$ and expand the time–dependent many–body state evolving from the equilibrium state $|G\rangle$ following photoexcitation. The time–dependence of the lattice coordinates is described by $M_l \frac{d^2 Q_l}{dt^2} = F_l(Q)$, where the forces are determined by the time–dependent populations $f_E(t)(t)$ of the above many–body eigenstates

$$F_l(Q,t) \approx -\frac{\partial}{\partial Q_l} \left[U_L(Q) + \langle G|H(Q)|G\rangle \right] - \sum_{E \neq G} f_E(t) \frac{\partial \varepsilon_E(Q)}{\partial Q_l}, \tag{29}$$

where

$$\varepsilon_E(Q) = \langle E|H(Q)|E\rangle - \langle G|H(Q)|G\rangle \tag{30}$$

are the e–h quasi–particle excitation energies. The latter are described by Fig. (3) and depend on the lattice displacement $Q(t)$. The first term on the rhs of Eq.(29) gives the adiabatic potential, which determines the lattice motion in the case of adiabatic time evolution of the insulating ground state $|G\rangle$ of $H(Q)$ without quasi–particle excitation.[30] The second term on the rhs of Eq.(29) describes a quasi–instantaneous change in the lattice potential and forces when the population of excited many–body states $|E\rangle$ becomes significant. Such non–equilibrium potential change initiates lattice motion following quasi–particle excitation and changes with time as determined by the evolution of the non–equilibrium populations $f_E(t)$ and by the dependence of the excitation

energies Eq.(30) on $Q(t)$. This is analogous to previous results in VO_2[54,60] and semiconductors.[51] A phase transition is triggered if $Q(t) \leq Q_c(t)$ during the lattice motion $Q(t)$, which can involve both coherent phonon oscillations and/or anharmonic lattice motion. Fig. (3) indicates a nonlinear Q–dependence of both ground state energy and e–h quasi–particle excitation energies, so Eq.(29) implies that the effective spring constants which determine, e.g., the coherent phonon oscillation frequencies, will change from their quasi–equilibrium values following photoexcitation of excited populations $f_E(t)$. On the other hand, for $E_{JT}(Q) \gg t$, the energy band Q–dependence is approximately linear, which implies much smaller changes in the sping constants. The fs–resolved XRD experimental results of Ref.[32] show that the photocarrier density transiently modifies the lattice spring constants in the manganites.

The laser–induced changes in the lattice potential and forces with quasi–particle excitation will initiate a lattice motion that depends on both $f_E(t)$ and $\frac{\partial \varepsilon_E(Q)}{\partial Q}$. New metastable quasi–equilibrium lattice configurations $Q_{eq}(t)$ can be obtained from Eq.(29) by setting $F_l(Q) = 0$. Such configurations depend on the elastic potential $U_L(Q)$, determined by multiple lattice modes and lattice anharmonicities.[30,58] For our purposes here, we assume for simplicity that $U_L(Q) = \frac{1}{2}kQ^2$. In this case, Eq.(29) gives quasi–equilibrium lattice configurations that depend on the photocarrier density:

$$Q_{eq}(t) = -\frac{1}{k}\frac{\partial}{\partial Q}\langle G|H(Q)|G\rangle - \frac{1}{k}\sum_{E \neq G} f_E(t)\,\frac{\partial \varepsilon_E(Q)}{\partial Q}. \qquad (31)$$

The first term determines the equilibrium lattice distortions, which are modified following photoexcitation of the continuum of many–body states $|E\rangle$. From Fig. (3) we see that $\frac{\partial \varepsilon_E(Q)}{\partial Q} > 0$ is dominated by the hole contribution to the excitation energy. The photoexcited quasi–particle populations then decrease the quasi–equilibrium lattice displacements to $Q_{eq}(t)$ during timescales where $f_E(t) \neq 0$. The latter lattice displacement changes with time as determined by the non–thermal electronic populations, which can lead to time–dependent changes in the hoppping amplitudes $\Delta V(t)$ as discussed above. The lattice displacements $Q_{eq}(t)$ are expected to be small, $Q_{eq}(t) \ll Q$, as compared to equilibrium in the case of laser–induced population inversion between the two different quasi–particle bands of Fig. (3). This is the case as the conduction and valence band eigenstates have different admixture of corner and bridge site configurations, which leads to their different Q–dependence. It may lead to an irreversible transition when $Q_{eq}(t) \leq Q_c(t)$.

The above picture of a photoinduced insulator to metal transition above a critical photocarrier density such that $Q(t) \leq Q_c(t)$ may be validated by experimental observations of nonlinear and threshold dependences of the ultrafast spectroscopy signals with increasing pump fluence and with a better temporal resolution that can distinguish between instantaneous and time–delayed processes. In the non–thermal temporal regime of interest here, a laser–induced population inversion between the polaronic–like majority carriers and the metallic–like minority carriers drives a nonlinear inter–dependence of spin, charge, and lattice dynamics. In this way, fs laser excitation can break the balance between electronic/magnetic and lattice degrees of freedom based on their different dynamics discussed above. To test this experimentally, one must be able to non–thermally control the quasi–particle populations while simultaneously monitoring the resulting spin, charge, and lattice time evolution on a fs timescale. This may be possible by using X–ray pulses[32,38] as their time resolution improves.

5. CONCLUSIONS

To conclude, in this paper we described a possible mechanism for photoinduced insulator to metal and AFM to FM simultaneous transitions triggered by non–thermal quasi–particle populations of a metallic conduction band. This mechanism involves non–adiabatic and nonlinear spin–charge–lattice coupling in the case of an AFM ground state consisting of FM chains and planes with JT distortions that stabilize the insulator energy gap. We propose that this mechanism may be relevant to explain the nonlinear pump fluence threshold dependencies of both magneto–optical (MOKE and MCD) and $\Delta R/R$ femtosecond signals measured in the PCMO manganite.[49] It may also be relevant to several other ultrafast spectroscopy experimental observations of nonlinear behavior during the non–thermal temporal regime following fs laser excitation of the AFM state of different insulating manganites.[17,18,32,33,34,35,36,37,38,39,40] In particular, we predict that electron–spin correlation leads to a broad conduction metallic band and quenches the electronic component of the insulator energy gap below a critical value

of the JT lattice displacement that depends on the photoexcitation. Such laser–induced effects are pronounced in the case of composite fermion quasi–particles with "soft" energy bands, which mostly populate the lower magnetic Hubbard band due to the large Hund's rule interaction and excite spin flucuations that lower their energy during electronic hopping timescales. Photoinduced FM correlation and spin canting following composite fermion quasi–particle photoexcitation instantaneously increases the critical lattice displacement $Q_c(t)$ below which the energy gap closes and leads to a metal–insulator phase transition that is also facilitated by the non–instantaneous relaxation of the JT distortions. In particular, above a critical photocarrier density, $Q_c(t)$ can become comparable to the equilibrium lattice distortion, while the latter decreases following lattice motion. Both effects act cooperatively to induce non–equilibrium insulator to metal and AFM to FM simultaneous transitions. We showed that FM correlation can develop instantaneously, so it can induce an instantaneous insulator to metal transition if $Q_c(t) \geq Q(t)$ during the laser pulse. Otherwise, lattice relaxation or oscillation is also required so that $Q(t)$ decreases. The excitation of multiple quasi–particles should increase the above nonlinearities by enhancing the deformation of the AFM background. After such excited quasi–electrons have relaxed on a fs timescale (τ^{fs}), electron–lattice and spin–lattice relaxation determines the subsequent ps dynamics (τ^{ps}).

The above theoretical framework may be relevant for explaining several experimental observations when worked cooperatively with lattice deformation and free energy quasi–equilibrium effects. The observation of a time–dependent spring constant[32] and nonlinear dependence of the coherent phonon amplitudes on the pump intensity during non–thermal fs timescales are consistent with "soft" quasi–particle energy bands such as the ones proposed here. Such bands of composite fermion quasi–particles make it easier to obtain a quasi–instantaneous insulator to metal and AFM to FM transitions as compared to bare electrons adiabatically decoupled from the spin background and nonlinear dependence of the coherent phonon amplitudes on the pump intensity during non–thermal fs timescales. In the latter case, the mechanism must rely on a more elaborate non–instantaneous lattice motion[53] in order to close the energy gap. In addition, a complex energy landscape, possibly with multiple local minima due to the elastic lattice potential $U_L(Q)$,[32,58] should facilitate the phase transition mechanism proposed here by increasing Q_c and creating metastable states. The insights from our theory, accompanied with relevant experiment results,[49] may also prove useful for revealing the crucial many–body processes in other intertwined electronic phases, as the proximity of magnetic states appears ubiquitous with unconventional superconducting and exotic electronic phases in strongly correlated electronic materials.[20] In the long run, new insights can be gained by applying complementary ultrafast spectroscopy techniques, especially in the terahertz[61] and infrared spectral regions,[62] and by combining spin and charge quantum fluctuations with quasi–equilibrium free energy and self–energy effects.

REFERENCES

[1] D. S. Chemla, and J. Shah, Nature **411**, 549 (2001).

[2] V. M. Axt, and S. Mukamel, Rev. Mod. Phys. **70**, 145 (1998).

[3] M. E. Karadimitriou, E. G. Kavousanaki, K. M. Dani, N. A. Fromer, and I. E. Perakis, J. Phys. Chem. B **115**, 5634 (2011); M. E. Karadimitriou, E. G. Kavousanaki, I. E. Perakis, and K. M. Dani, Phys. Rev. B **82**, 165313 (2010).

[4] T. Li, A. Patz, L. Mouchliadis, J. Yan, T. A. Lograsso, I. E. Perakis, and J. Wang, Nature **496**, 69 (2013).

[5] T. Papenkort, T. Kuhn, and V. M. Axt, Phys. Rev. B 78, 132505 (2008); R. Matsunaga, Y. I. Hamada, K. Makise, Y. Uzawa, H. Terai, Z. Wang, and R. Shimano, Phys. Rev. Lett. 111, 057002 (2013).

[6] J. Bigot, M. Vomir, and E. Beaurepaire, Nature Physics **5**, 515 (2009).

[7] P. C. Lingos, J. Wang, and I. E. Perakis Phys. Rev. B 91, 195203 (2015); M. D. Kapetanakis, P. C. Lingos, C. Piermarocchi, J. Wang, and I. E. Perakis, Appl. Phys. Lett. **99**, 091111 (2011); M. D. Kapetanakis, I. E. Perakis, K. J. Wickey, C. Piermarocchi, and J. Wang, Phys. Rev. Lett. **103**, 047404 (2009).

[8] M. Porer, U. Leierseder, J.-M. Mnard, H. Dachraoui, L. Mouchliadis, I. E. Perakis, U. Heinzmann, J. Demsar, K. Rossnagel, and R. Huber, Nature Materials **13**, 857 (2014).

[9] P. Koskinen and V. Mkinen, Density-functional tight-binding for beginners, Computational Materials Science **47**, 237 (2009).

[10] B. Lazarovits, K. Kim, K. Haule, and G. Kotliar, Effects of strain on the electronic structure of VO2, Phys. Rev. B **81**, 115117 (2010).

[11] J.P.F. LeBlanc, A. E. Antipov, F. Becca, I. W. Bulik, G. K.-L. Chan, C.-M. Chung, Y. Deng, M. Ferrero, T. M. Henderson, C. A. Jimnez-Hoyos, E. Kozik, X.-W. Liu, A. J. Millis, N.V. Prokofev, Mingpu Qin, G. E. Scuseria, H. Shi, B.V. Svistunov, L. F. Tocchio, I.S. Tupitsyn, S. R. White, S. Zhang, B.-X. Zheng, Z. Zhu, and E. Gull Phys. Rev. X **5**, 041041 (2015).

[12] I. E. Perakis and T. Shahbazyan, Surface Science Reports **40**, 1 (2000).

[13] E. Dagotto, T. Hotta, and A. Moreo, Phys. Rep. **344**, 1 (2001).

[14] Y.M. Sheu, S.A. Trugman, L. Yan, J. Qi, Q.X. Jia, A.J. Taylor, and R.P. Prasankumar, Phys. Rev. X **4**, 021001 (2014).

[15] H. Ichikawa, *et. al.*, Nature Mat., **10**, 2929 (2011).

[16] M.Fiebig, K. Miyano, Y Tomioka, and Y Tokura, Science **280**, 1925 (1998).

[17] D. Polli, M. Rini, S. Wall, R. W. Schoenlein, Y. Tomioka, Y. Tokura, G. Cerullo, and A. Cavalleri, Nature Mat. **6**, 643 (2007).

[18] M. Rini, R. Tobey, N. Dean, J. Itatani, Y. Tomioka, Y. Tokura, R. W. Schoenlein, and A. Cavalleri, Nature **449**, 72 (2007).

[19] G. C. Milward, M. J. Calderón, and P. B. Littlewood, Nature **433**, 607 (2005).

[20] A. Patz, T. Li, S. Ran, R. M. Fernandes, J. Schmalian, S. L. Budko, P. C. Canfield, I. E. Perakis, and J. Wang, Nat. Commun. **5**, 3229 (2014).

[21] S. G. Ovchinnikov and V. V. Valkov, *Hubbard Operators in the Theory of Strongly Correlated Electrons*, Imperial College Press (London, 2004).

[22] A. E. Ruckenstein and S. Schmitt-Rink, Phys. Rev. B **38**, 7188(R) (1988).

[23] V. M. Loktev and Yu. G. Pogorelov, Low Temp. Phys. **26**, 171 (2000).

[24] V. Ramakrishnan, H. R. Krishnamurthy, S. R. Hassan, and G. Venketeswara Pai, Phys. Rev. Lett. **92**, 157203 (2004); O. Cepas, H. R. Krishnamurthy, and T. V. Ramakrishnan, Phys. Rev. B **73**, 035218 (2006).

[25] T. V. Ramakrishnan, J. Phys. Condens. Matter **19**, 125211 (2007).

[26] D. Basov, R. D. Averitt, M. Dressel, D. Vandermarel, and K. Haule, Rev. Mod. Phys. **83**, 471 (2011).

[27] A. J. Millis, P. B. Littlewood, and B. I Shraiman, Phys. Rev. Lett. **74**, 5144 (1995).

[28] K. I. Kugel, A. L. Rakhmanov, and A. O. Sboychakov, Phys. Rev. Lett. **95**, 267210 (2005); A. O. Sboychakov, K. I. Kugel, and A. L. Rakhmanov, Phys. Rev. B **74**, 014401 (2006).

[29] D. Wegkamp and J. Stahler, Progress in Surface Science **90**, 464 (2015).

[30] A. Subedi, A. Cavalleri, and A. Georges, Phys. Rev. B **89**, 220301(R) (2014).

[31] V. R. Morrison, R. P. Chatelain, K. L. Tiwari, A. Hendaoui, A. Bruhacs, M. Chaker, and B. Siwick, Science 346, 445 (2014).

[32] P. Beaud, A. Caviezel, S. O Mariager, L. Rettig, G. Ingold, C. Dornes, S.-W. Huang, J. A. Johnson, M. Radovic, T. Huber, T. Kubacka, A. Ferrer, H. T. Lemke, M. Chollet, D. Zhu, J. M. Glownia, M. Sikorski, A. Robert, H. Wadati, M. Nakamura, M. Kawasaki, Y. Tokura, S. L. Johnson, and U. Staub, Nature Materials **13**, 923 (2014).

[33] M. Forst, R. I. Tobey, S. Wall, H. Bromberger, V. Khanna, A. L. Cavalieri, Y.-D. Chuang, W. S. Lee, R. Moore, W. F. Schlotter, J. J. Turner, O. Krupin, M. Trigo, H. Zheng, J. F. Mitchell, S. S. Dhesi, J. P. Hill, and A. Cavalleri, Phys. Rev. B **84**, 241104(R) (2011).

[34] K. Miyasaka, M. Nakamura, Y. Ogimoto, H. Tamaru, and K. Miyano, Phys. Rev. B **74**, 012401 (2006).

[35] M. Matsubara, Y. Okimoto, T. Ogasawara, Y.Tomioka, H. Okamoto, and Y. Tokura, Phys. Rev. Lett. **99**, 207401 (2007).

[36] Y. Okimoto, H. Matsuzaki, Y. Tomioka, I. Kezsmarki, T. Ogasawara, M. Matsubara, H. Okamoto, and Y. Tokura, J. Phys. Soc. Jpn. **76**, 043702 (2007).

[37] S. Wall, D. Prabhakaran, A. T. Boothroyd, and A. Cavalleri, Phys. Rev. Lett. **103**, 097402 (2009).

[38] H. Ehrke, R. I. Tobey, S. Wall, S. A. Cavill, M. Forst, V. Khanna, Th. Garl, N. Stojanovic, D. Prabhakaran, A. T. Boothroyd, M. Gensch, A. Mirone, P. Reutler, A. Revcolevschi, S. S. Dhesi, and A. Cavalleri, Phys. Rev. Lett. **106**, 217401 (2011).

[39] H. Matsuzaki, H. Uemura, M. Matsubara, T. Kimura, Y. Tokura, and H. Okamoto, Phys. Rev. B **79**, 235131 (2009).

[40] R. Singla, A. Simoncig, M. Frst, D. Prabhakaran, A. L. Cavalieri, and A. Cavalleri, Phys. Rev. B 88, 075107 (2013).

[41] M. D. Kapetanakis and I. E. Perakis, Phys. Rev. Lett. **101**, 097201 (2008); Phys. Rev. B **78**, 155110 (2008).

[42] M. D. Kapetanakis and I. E. Perakis, Phys. Rev. B **75**, 140401(R) (2007); M. D. Kapetanakis, A. Manousaki, and I. E. Perakis Phys. Rev. B 73, 174424 (2006).

[43] F. Ye, P. Dai, J. A. Fernandez-Baca, H. Sha, J. W. Lynn, H. Kawano-Furukawa, Y. Tomioka, Y. Tokura, and J. Zhang, Phys. Rev. Lett. 96, 047204 (2006); F. Ye, P. Dai, J. A. Fernandez-Baca, D. T. Adroja, T. G. Perring, Y. Tomioka, and Y. Tokura, Phys. Rev. B 75, 144408 (2007).

[44] J. C. Hubbard, Proc. Roy. Soc. A **276**, 238 (1963); *ibid* **281**, 401 (1964); *ibid* **285**, 542 (1965).

[45] F. C. Zhang and T. M. Rice, Phys. Rev B **37**, 3759 (1988)

[46] Y. Tokura and N. Nagaosa, Science 288, 462 (2000).

[47] S. Yunoki, T. Hotta, and E. Dagotto, Phys Rev. Lett. 84, 3714 (2000).

[48] A. Takahashi and S. Mukamel, J. Chem. Phys. **100**, 2366 (1994).

[49] P. C. Lingos, A. Patz, T. Li, G. D. Barmparis, A. Keliri, M. D. Kapetanakis, L. Li, J. Yan, J. Wang, and I. E. Perakis, Phys. Rev. **B 95**, 224432, (2017).

[50] P. W. Anderson and H. Hasegawa, Phys. Rev. **100**, 675 (1955); P.–G. de Gennes, Phys. Rev. **118**, 141 (1960).

[51] H. J. Zeiger, J. Vidal, T. K. Cheng, E. P. Ippen, G. Dresselhaus, and M. S. Dresselhaus, Phys. Rev. B **45**, 768 (1992).

[52] A. Daoud–Aladine *et. al.*, Phys. rev. lett. **89**, 097205 (2002); D. Garcia *et. al.*, Phys. Rev. Lett. **85**, 3720 (2000); C. I. Ventura and B. Alascio, Phys. Rev. B **68**, 020404(R) (2003).

[53] M. van Veenedaal, Phys. Rev. B **94**, 115101 (2016).

[54] Z. He and A. J. Millis, Phys. Rev. B **93**, 115126 (2016).

[55] V. Ferrari, M. Towler, and P. B. Littlewood, Phys. Rev. Lett. **91**, 227202 (2003)

[56] A. Tanaka, J. Phys. Soc. Japan **72**, 2433 (2003); ibid **73**, 152 (2004).

[57] J. van der Brink, G. Khaliullin, and D. Khmoskii, Phys. Rev. Lett. **83**, 5118 (1999).

[58] K. H. Ahn, T. Lookman, and A. R. Bishop, Nature **428**, 401 (2004); K. H. Ahn, T. F. Seman, T. Lookman, and A. R. Bishop, Phys. Rev. B **88**, 144415 (2013).

[59] T. N. Todorov, J. Phys. Condens. Matter. **13**, 10125 (2001).

[60] M. van Veenendaal, Phys. Rev. B **87**, 235118 (2013).

[61] L. Luo, I. Chatzakis, A. Patz, and J. Wang, Phys. Rev. Lett. **114**, 107402 (2015); L. Luo, I. Chatzakis, J. Wang, F. B. P. Niesler, M. Wegener, T. Koschny, and C. M. Soukoulis, Nat. Commun. **5**, 3055 (2014); I. Chatzakis, L. Luo, J. Wang, N.-H. Shen, T. Koschny, J. Zhou, and C. M. Soukoulis, Phys. Rev. B **86**, 125110 (2012).

[62] J. Wang, M. W. Graham, Y. Ma, G. R. Fleming, and R. A. Kaindl, Phys. Rev. Lett. **104**, 177401 (2010); T. Li, L. Luo, M. Hupalo, J. Zhang, M. C. Tringides, J. Schmalian, and J. Wang, Phys. Rev. Lett. **108**, 167401 (2012); J. Wang, G. A. Khodaparast, J. Kono, A. Oiwa, and H. Munekata, J. of Mod. Opt. **51**, 2771 (2004); J Wang, GA Khodaparast, J Kono, T Slupinski, A Oiwa, H Munekata, Journal of superconductivity, **16**, 373 (2003).